Experimental investigation and modelling of hydrodynamics and heat transfer in flow boiling in normal and microgravity conditions

Paul Onubi Ayegba, Julien Sébilleau, Catherine Colin

International Journal of Multiphase Flow 181 (2024) 104991

Contents lists available at ScienceDirect

International Journal of Multiphase Flow

journal homepage: www.elsevier.com/locate/ijmulflow

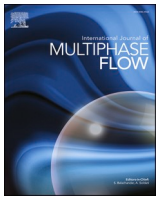

Experimental investigation and modelling of hydrodynamics and heat transfer in flow boiling in normal and microgravity conditions

Paul Onubi Ayegba, Julien Sebilleau, Catherine Colin *

Institut de Mécanique des Fluides de Toulouse – Université de Toulouse – CNRS-INPT-UPS, Allée Camille Soula 31400 Toulouse France

ARTICLE INFO

Keywords:
Microgravity
Upward flow
Downward flow
Flow boiling
Flow patterns
Heat transfer coefficient
Modelling

ABSTRACT

The development of long-term space thermal management systems has informed research into the influence of gravity on boiling. This work explored the influence of gravity on the hydrodynamics and heat transfer of boiling flow. Experiments were carried out using two test loops each consisting of a 6 mmID transparent cylindrical test section. Upward ($+1g$) and downward ($-1g$) flow boiling experiments were carried out in the laboratory while microgravity (μg) experiments were carried out during a parabolic flight campaign. The results of flow visualisation showed significant influence of gravity on the flow patterns and the influence of gravity was generally limited to mass flux, $G \leq 400\ kg/m^2s$ and/or vapor quality, $x \leq 0.35$. In all three gravity conditions, the measured heat transfer coefficient was influenced by heat flux, mass flux and/or vapor quality. For liquid Reynolds number, $Re_{lo} \leq 2000$ $(G \leq 150\ kg/m^2s)$ and boiling number $Bo < 0.002$ the measured heat transfer coefficient was highest in $-1g$ flow and lowest in μg flow but becomes comparable at $Bo > 0.002$. A correlation for predicting microgravity heat transfer coefficient was proposed in this work and the proposed correlation predicted 100 % of the μg data in the current work within ±20%, predicted nearly 100 % of the μg data of Ohta et al. (2013) within ±30% and around 85 % of the μg data of Narcy (2014) within -20 % to +50 %. A correlation for predicting the gravity dependent regime as it relates to heat transfer coefficient in $+1g$ and μg flows was also proposed in this work. The proposed criterium correctly predicted over 85 % of the gravity-dependent heat transfer coefficient in the current work and the works of Lebon et al. (2019), Narcy (2014), Ohta et al. (2013).

1. Introduction

Flow boiling applications operating under various gravity conditions are common in avionics, power plants and various space applications. Gravity strongly influences flow patterns and heat transfer coefficient. Flow boiling has been mainly studied in vertical upward flows (1-*g*) in both subcooled and saturated boiling conditions. Review articles on flow boiling heat transfer provide references and analyses of experimental data, mechanistic models and empirical correlations in the nucleate and convective boiling regimes (Cioncolini and Thome, 2011; Hong et al., 2023; Kandlikar, 1990; Kim and Mudawar, 2013; Narcy and Colin, 2015). In flow boiling, both nucleate boiling (evaporation and quenching) and convective boiling (two-phase forced convection) contribute to total heat transfer. Therefore, correlations for flow boiling heat transfer coefficient are often expressed as a weighted average of the contributions of each of these mechanisms. Nucleate boiling is prominent in the bubbly and slug flow regimes and is also a feature in the annular flow regime for low liquid velocity and/or high wall heat flux. Nucleate boiling heat transfer (h_{nb}) increases with the heat flux due to bubble nucleation. Convective boiling is prominent in annular flows especially at high velocity and/or low heat flux. The convective heat transfer (h_{cb}) increases with vapour quality due to thinning of the annular liquid film (Kim and Mudawar, 2013).

Experiments have also been performed in downward flow (-1*g*) (Ayegba et al., 2022; Kharangate et al., 2016) and in microgravity conditions (Baltis et al., 2012; Celata and Zummo, 2009; Hong et al., 2023; Lebon et al., 2019; Luciani et al., 2009; Ma and Chung, 2001; Mudawar and Lee, 2023; Narcy et al., 2014; Ohta, 1997). Results of these studies include flow patterns and heat transfer measurements. The results are often compared to $+1g$ upward flow data. Flow orientation or gravity level have been reported to influence both flow patterns and flow pattern transition (Bhagwat and Ghajar, 2012; Celata and Zummo, 2009; Godbole et al., 2011), as well as heat transfer coefficient. It can be concluded from available experimental data in microgravity (μg) and

* Corresponding author.
E-mail address: catherine.colin@imft.fr (C. Colin).

https://doi.org/10.1016/j.ijmultiphaseflow.2024.104991
Received 20 April 2024; Received in revised form 14 August 2024; Accepted 5 September 2024
Available online 7 September 2024

normal gravity ($+1g$, $-1g$) flows that, flow boiling heat transfer increases with wall heat flux, especially in the nucleate boiling dominant regime (Baba et al., 2012; Lebon et al., 2019; Mudawar and Lee, 2023; Narcy et al., 2014). Below critical heat flux and in the convective boiling dominant regime, saturated flow boiling heat transfer generally increases with vapor quality and is independent of gravity level/flow orientation relative to gravity at higher vapor quality (Ayegba et al., 2022; Baba et al., 2012; Konishi and Mudawar, 2015). Despite the numerous studies in microgravity, to our knowledge, no model has been proposed to predict heat transfer coefficient.

In the subcooled and/or nucleate boiling regime(s), reports on the effect of flow direction relative to gravity on flow boiling heat transfer are limited. In the work of Baba et al. (2012), which was done using FC-72 inside 0.51 *mm* tube, they reported higher subcooled heat transfer coefficient in downward flows ($-1g$) relative to upward flows ($+1g$) $h_{-1g} > h_{+1g}$. Kharangate et al. (2016), in their channel (5.0 *mm* × 2.5 *mm*) flow measurements, using FC-72, reported equivalent subcooled heat transfer coefficient in both upward and downward flows $h_{-1g} \approx h_{+1g}$. With regards to the effect of gravity levels, available results are rather conflicting. Iceri et al. (2020), Luciani et al. (2009, 2008) and Lui et al. (1994) all reported higher subcooled heat transfer coefficient in microgravity flow (μg) relative to upward flow ($+1g$) in their parabolic flight and ground experiments ($h_{\mu g} > h_{+1g}$). Similar result was reported by Baltis et al. (2012) for $G \geq 150 kg/m^2 s$ ($D = 6\ mm$, $h_{\mu g} > h_{+1g}$). However, they reported lower subcooled heat transfer coefficient in μg relative to $+1g$ for $G \leq 100 kg/m^2 s$. On the other hand, Ohta (1997) and Saito et al. (1994) both reported equivalent subcooled heat transfer in μg and $+1g$ ($h_{\mu g} \approx h_{+1g}$). Other investigations reported higher heat transfer coefficient in $+1g$ relative to μg (Celata, 2007; Konishi et al., 2015; Lebon et al., 2019; Trejo-Peimbert, 2018).

In the saturated and/or convective boiling regime(s), the limited studies report little or no influence of gravity on the heat transfer coefficient. While Baba et al. (2012) reported slightly higher saturated heat transfer in downward flow relative to upward flow, Kharangate et al. (2016) reported equivalent saturated heat transfer coefficient in both flow directions ($h_{-1g} \approx h_{+1g}$) particularly for $G \geq 800 kg/m^2 s$. With respect to the influence of gravity levels on heat transfer in the convective boiling dominant regime, Celata (2007) and Luciani et al. (2009, 2008) reported similar saturated heat transfer in μg and $+1g$ ($h_{\mu g} \approx h_{+1g}$). However, Ohta (1997) reported lower saturated heat transfer coefficient in microgravity relative to normal gravity.

Several studies have attempted to provide criteria for gravity-dependence of the heat transfer coefficient based on the mixture Froude number Fr_m, heat flux and mass flux (Lebon et al., 2019) or a combination of mass flux, heat flux and vapor quality (Ohta et al., 2013). The proposed gravity dependence map of Lebon et al. (2019) was derived from low-mass-flux data, where nucleate boiling (NB) was the dominant mechanism of heat transfer. They provided upper limits of wall heat flux (q'') for various mass fluxes at which the measured heat transfer coefficient becomes independent of gravity. The gravity-dependence criterium of Baba et al. (2012) applies to flow boiling where convective heat transfer is dominant. According to Baba et al. (2012), flow boiling heat transfer coefficient becomes independent of gravity if the mixture Froude number $Fr_m \geq 4$ (Eq. (1). The criteria proposed by Ohta et al. (2013) captures all the relevant macro quantities reported to determine gravity-dependence, but like Lebon et al. (2019), it was provided in the form of a dimensional gravity-dependence regime map. Their gravity-dependence map highlighted limits of heat flux, mass flux and vapor quality where gravity influence was observed.

$$Fr_m = \frac{inertia}{bouyancy} = G \Big/ \sqrt{\rho_m(\rho_l - \rho_v)gD} \tag{1}$$

where $\rho_m = \frac{1}{x/\rho_v + (1-x)/\rho_l}$, ρ_l, ρ_v, g and D are the liquid density, vapor density, acceleration due to gravity and hydraulic diameter respectively.

In the current work, new experimental data obtained in microgravity are presented, focusing on the flow patterns and heat transfer coefficient under various conditions of mass flux, wall heat flux and vapor quality. These results are compared to previous results obtained $+1g$ and $-1g$ flows (Ayegba et al., 2022). The experimental data will be used to describe the gravity dependent regimes as well as the nucleate and convective dominant regimes. Also, correlations for predicting microgravity heat transfer coefficient in both subcooled and saturated boiling regimes will be provided in this work. The proposed correlation will be validated using experimental data from the current work as well as selected data from literature (Ayegba et al., 2022; Narcy, 2014; Ohta et al., 2013).

2. Experimental Setup and measurement techniques

The experimental aspect of this work involves flow visualization along with the measurement of heat transfer coefficient in a vertical tube of 6 *mmID* and 8 *mmOD* in μg, $+1g$ and $-1g$ using HFE-7000 as working fluid (Table 1). Two flow loops were used namely BRASIL (Ayegba et al., 2022; Narcy et al., 2014) and COSMO (Chorin et al., 2023) in the present study (Fig. 1). The BRASIL loop was used in the lab to study upward and downward flow boiling in a vertical tube. A second loop COSMO, more compact, was built in 2021, specifically for microgravity experiments in parabolic flights. Due to the smaller size of the loop a specific design has been performed to assess the axisymmetric of the flow in the test section both in single phase flow with PIV measurements and in bubbly flow with 3D visualizations of the bubble distribution in the tube cross section (Chorin et al., 2023). Some sets of experiments were performed in 1g upward flow with BRASIL and COSMO to show the consistency of the measurement techniques. In both loops, preheated single-phase liquid or two-phase vapor-liquid flow enters the transparent Sapphire tube test section at pressures which can be varied from 1 to 2 bar ($34^oC < T_{sat} < 54^oC$). Further heating of the fluid was done by resistive heating using an indium-tin-oxide (ITO) coating on the outer wall of the Sapphire tube, to which a voltage source is connected. The thickness of the ITO coating was 100 nm, and the coated length was 180 mm. In general, an outlet vapor quality of up to 0.9 can be attained in both BRASIL and COSMO setups depending on the mass flux. Fluid exiting the test section is condensed and cooled to the desired temperature at the inlet of the pump using Peltier module(s) in the condenser. Peltier module power regulation was automated and driven by a PID which sets the liquid temperature at the pump inlet. The pump inlet temperatures were set to $\leq T_{sat} - 10^oC$ to avoid cavitation. In this study, mass fluxes of 50,75,100,200 and 400 $kg.m^{-2}s^{-1}$ were studied using BRASIL ($+1g$ and $-1g$) and mass fluxes of 50,75,100 and 150 $kg.m^{-2}s^{-1}$ were investigated using the COSMO setup ($+1g$ and μg). The heat fluxes ranged between 0.5 W/cm^2 and 3 W/cm^2 depending on the flow rate (Table 2).

The microgravity experiments were carried out onboard the Airbus A310 ZERO-G aircraft managed by Novespace in collaboration with the French Space Agency (CNES) and the European Space Agency (ESA). A series of 93 parabolas (31 each day) were done over a 3-day flight campaign. Each parabolic maneuver included a hyper gravity phase of 20 s at $(+1.8g)$, followed by the microgravity period (μg) of about 22 s

Table 1
Properties of HFE-7000 at 25°C and atmospheric pressure.

Property	Value
Molecular weight	200 g/mol
Saturation temperature	34 °C
Liquid density	1400 kg/m^3
Vapour density	8 kg/m^3
Thermal conductivity	0.075 $W/m/K$
Kinematic Viscosity	$3.2 \times 10^{-7} m^2/s$
Specific Heat	1300$J/kg/K$
Surface Tension	0.0124 N/m
Latent Heat of Vaporization	127 kJ/kg

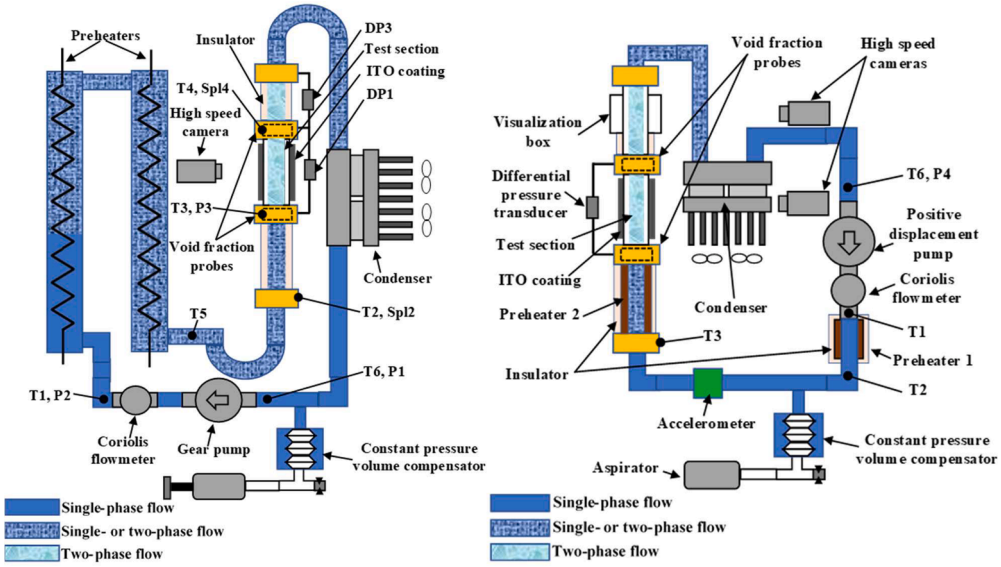

Fig. 1. Sketch of the BRASIL experimental flow loop (left) and COSMO experimental flow loop (right).

Table 2
Test conditions: $1.2 \leq P \leq 1.5\ bar$, $15 \leq \Delta T_{sub} \leq 5$, $0 \leq x_{in} \leq 0.3$.

	Upward flow	Microgravity flow	Downward flow
$G \approx 50\ kg/m^2s$	$0.5 \leq q_w \leq 2.0\ W/cm^2$	$0.5 \leq q_w \leq 1.5\ W/cm^2$	$0.5 \leq q_w \leq 1.5\ W/cm^2$
$G \approx 75\ kg/m^2s$	$1.0 \leq q_w \leq 3.0\ W/cm^2$	$0.5 \leq q_w \leq 2.0\ W/cm^2$	$0.5 \leq q_w \leq 2.0\ W/cm^2$
$G \approx 100\ kg/m^2s$	$1.0 \leq q_w \leq 3.0\ W/cm^2$	$0.5 \leq q_w \leq 2.0\ W/cm^2$	$0.75 \leq q_w \leq 2.0\ W/cm^2$
$G \approx 150\ kg/m^2s$	-	$0.5 \leq q_w \leq 2.0\ W/cm^2$	-
$G \approx 200\ kg/m^2s$	$1.0 \leq q_w \leq 3.0\ W/cm^2$	-	$1.0 \leq q_w \leq 3.0\ W/cm^2$
$G \approx 400\ kg/m^2s$	$1.5 \leq q_w \leq 3.0\ W/cm^2$	-	$1.5 \leq q_w \leq 3.0\ W/cm^2$

and a second hyper gravity phase of 20 s at ($+$ 1.8g). 2 consecutive parabolas are separated by a horizontal steady flight ($+1g$) for 2 minutes. Although data acquisition was done for nearly the entire 22 s of μg condition, only mean value for the last 10 s was used in data post-processing. This was because the relevant flow parameters such as the wall temperature, pressure and flow rate typically stabilize only after the first 10 s of the μg flight maneuver (Fig. 2).

Diagnostics used include Coriolis flow meter, thermocouples, pressure transducers, and high-speed cameras (PCO Dimax, 2000×2000 pixels and PCO1200HS, 1280×1024 pixels). Details of the diagnostics, measurement technics, data reduction and uncertainties are available elsewhere (Ayegba et al., 2023, 2022; Chorin et al., 2023; Narcy et al., 2014). The quality (x) used in all plots is the flow quality (different from the thermodynamic quality in subcooled boiling) and details of how this was obtained is provided elsewhere (Ayegba et al., 2022; Narcy et al., 2014).

3. Experimental results

3.1. Flow patterns

Flow visualizations were carried out at various two-phase flow conditions ranging from subcooled to saturated boiling regimes for μg flow ((Fig. 3) and these were compared to flow visualizations of $+1g$ and $-1g$ flows. Over the entire range of mass fluxes in μg and $+1g$ flows, bubbly, intermittent (slug, churn and other transitions flows) and annular flow regimes were observed. Similar flow patterns were also observed for $-1g$ flow at $G/\rho_l \geq 0.15\ m/s$ $\left(G \geq 200 kg/m^2 s\right)$. Below this

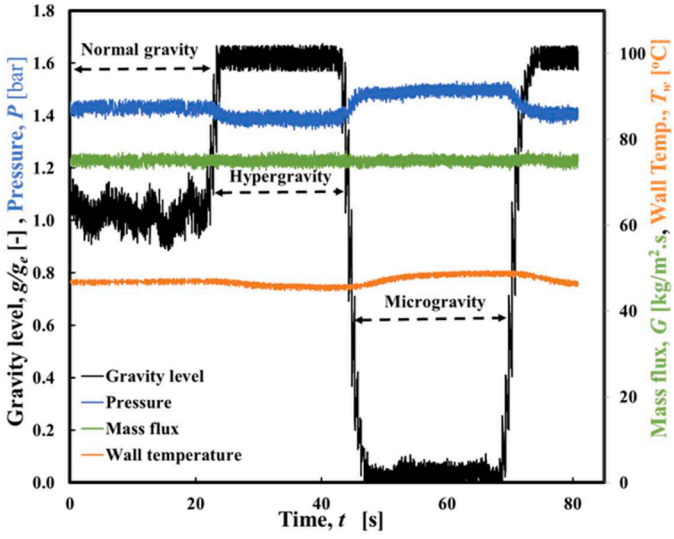

Fig. 2. Time evolution of mass flux, pressure and wall temperature under various gravity conditions in parabolic flight.

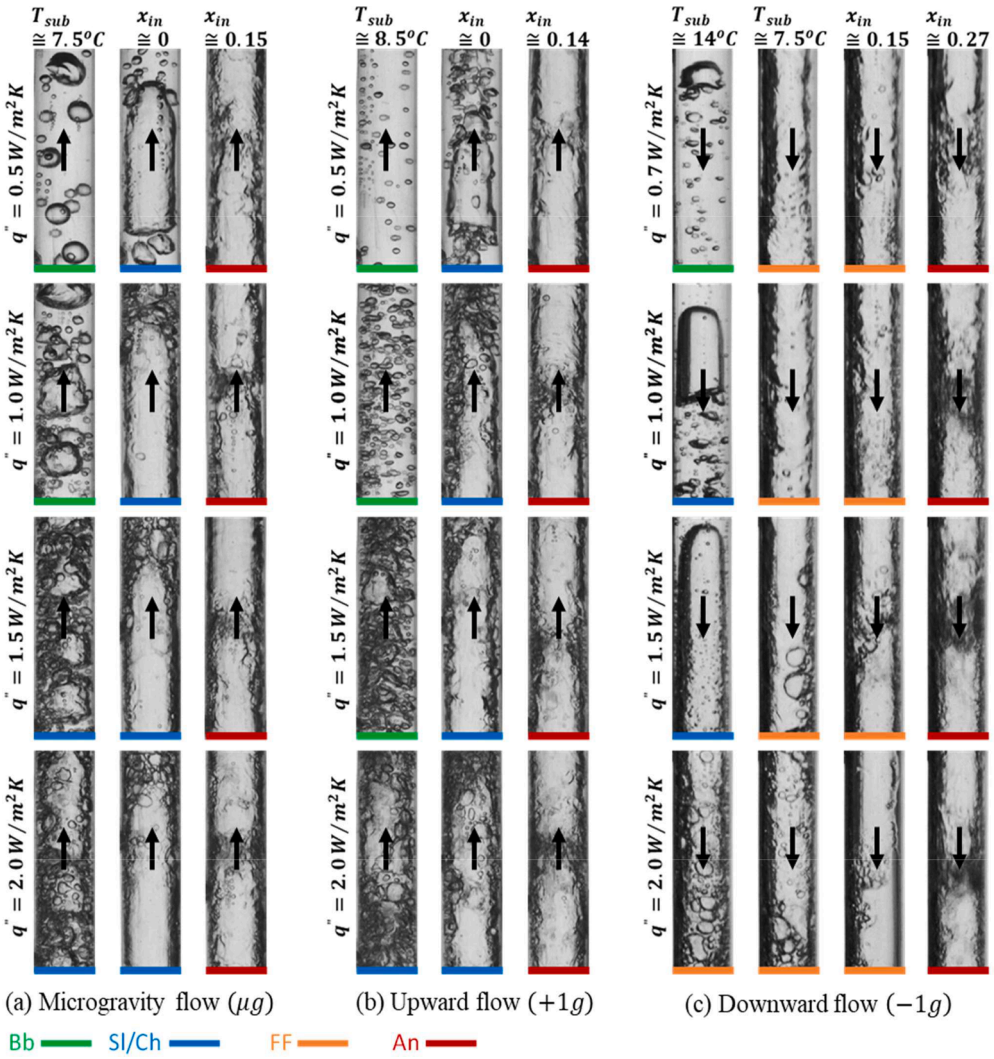

Fig. 3. Flow visualization in upward, microgravity and downward flows at $G/\rho_l = 0.075\ m/s$ $(G = 100kg/m^2s)$. The arrows indicate the direction of flow.

liquid velocity, bubbly and intermittent flow regimes were replaced by falling-film flow regime in $-1g$ flow.

3.1.1. *Bubbly flow*

In general, mean bubble size in the bulk fluid decreased from $-1g$ flow through μg to $+1g$ in line with the bubble drift velocities associated with these gravity conditions (Fig. 3). Bubbles are mostly spherical in μg in absence of relative velocity, whereas they are ellipsoidal in $+1g$ and $-1g$.

In μg and $+1g$ flows, bubbly flow was observed at subcooled inlet conditions and low heat flux ($q'' \leq 1.5W/cm^2$) (Fig. 3a-b). The mean bubble sizes of both nucleated and entrained bubbles were significantly larger in μg relative to $+1g$ flow. The absence of buoyancy forces in the former results in longer residence of the bubbles both at the wall and in the bulk flow along with higher bubble coalescence in the bulk flow.

For $-1g$ flow, co-current bubbly flow was limited to $G/\rho_l \geq 0.15\ m/s$ $(G \geq 200kg/m^2s)$. At $G/\rho_l = 0.075\ m/s$ $(G = 100kg/m^2s)$, high subcooling ($T_{sub} > 10°C$) and low heat flux ($q'' \leq 1.0W/cm^2$), small detached bubbles moved upward while large coalesced bubbles, with bubble diameter ≈ tube diameter, moved downward ((Fig. 3c). This results in oscillating bubbly/intermittent flow. At $G/\rho_l < 0.075\ m/s$ (all heat fluxes) or $G/\rho_l = 0.075\ m/s$ ($q'' > 1.0W/cm^2$), the bubbly and intermittent flow regimes are replaced by a high-void-fraction falling-film regime. It should be remarked that the mean size of nucleated bubbles in $-1g$ was either similar or smaller than that in μg flow. While negative gravity may promote bubble attachment to the heated wall, the liquid velocity in $-1g$ is relatively higher than in μg and $+1g$ flows, thereby reducing the thickness of the thermal boundary layer. Conversely, the mean bubble size in the bulk fluid was significantly larger in $-1g$ flow relative to both μg and $+1g$ flows. This is due to the significantly higher residence time of bubble in the bulk fluid in the former.

Overall, the effect of gravity on bubble geometry becomes negligible at high mass fluxes (Ayegba et al., 2022; Narcy et al., 2014). Narcy et al. (2014) showed the difference in bubble geometry between μg and $+1g$ flows become negligible at $G/\rho_l \geq 0.4\ m/s$ $(G \geq 540kg/m^2s)$ while Ayegba et al. (2022) showed that the difference in bubble geometry between $+1g$ and $-1g$ flows become negligible at $G/\rho_l \geq 0.3\ m/s$ $(G \geq 400kg/m^2s)$.

3.1.2. *Intermittent flow*

At subcooled inlet conditions, increase in wall heat flux results in a transition from bubbly to churn flow in μg and $+1g$ flows as well as in $-1g$ flow for $G/\rho_l \geq 0.15\ m/s$ (Fig. 3). For $-1g$ flow at $G/\rho_l \leq 0.075\ m/s$, the flow pattern is either falling-film or changes from bubbly to falling-film with increase in wall heat flux.

At low heat flux ($q'' \leq 1.0W/cm^2$), decrease in inlet subcooling resulted in transition from bubbly to Taylor bubbles (slug flow) in μg and $+1g$ flows as well as in $-1g$ at $G/\rho_l \geq 0.15\ m/s$. Slug flow was predominant at very low inlet quality ($0 \leq x_{in} \leq 0.14$). The roughness of the

interface of the Taylor bubbles increased from $-1g$ flow through μg to $+1g$ in line with the respective drift velocities.

The falling-film regime in $-1g$ flow was characterized by low velocity vapor core and a thin liquid film flowing along the wall. The interface between the liquid film and vapor core is covered by ripples and free from roll waves.

3.1.3. Annular flow

In all three gravity conditions, increase in inlet vapor quality resulted in transition from intermittent to annular flow regime (Fig. 3). The annular flow regime was characterized by interfacial roll waves along with capillary waves. The vapor quality and/or void fraction at with such transition occurs, differs in function of the gravity levels.

3.1.4. Flow pattern map

Flow pattern maps along with comparisons with various transitions criteria for $+1g$ and $-1g$ flows were presented in Ayegba et al. (2022) and displayed in Fig. 4c and Fig. 4d respectively in terms of liquid and vapor superficial velocities. Experimental results in μg and $+1g$ flows were presented in (Narcy et al. (2014). In the current work, the flow pattern map obtained in μg and $+1g$ are plotted in Fig. 4a and Fig. 4b. Transition from bubbly to slug/churn flow is due to bubble coalescence and both regimes represent a continuum of the same physical process (Colin et al., 1991). For μg flows in the heated section, Narcy et al. (2014) reported a critical void fraction (α_c) for bubbly-slug transition of ≈ 0.70 while (Celata and Zummo, 2009), reported α_c of 0.74. In the current work the mean void fractions at transition from bubbly to slug flow were $\alpha_c \approx 0.65$, $\alpha_c \approx 0.68$ and $\alpha_c \approx 0.75$ for $+1g$, μg and $-1g$ flows, respectively.

Based on experimental data of vertical gas-liquid adiabatic flow in a 40 *mmID* tube, Colin et al. (1991), proposed a bubbly-slug transition criterium from the drift model with distribution coefficient C_0 of 1.2 and α_c of 0.45. In the current work C_0 of 1.15 provided better prediction of both the bubbly-slug transition boundary and the bubble velocity. In microgravity, the drift flux model is given by Eq. (2) and the corresponding vapor quality, x_c is given by Eq. (3).

$$u_v = \frac{j_v}{\alpha_c} = C_0 j \text{ or } j_l = \frac{1 - C_0\alpha_c}{C_0\alpha_c} j_v \tag{2}$$

$$x_c = \frac{1}{1 + \frac{1-C_0\alpha_c}{C_0\alpha_c}\frac{\rho_l}{\rho_v}} \tag{3}$$

where u_v is the vapor velocity, C_0 is the distribution coefficient, j_v, and j_l are the vapor and liquid superficial velocity, j is the mixture velocity, ρ_v and ρ_l are the vapor and liquid densities, α_c and x_c are the void fraction and vapor quality at transition.

Using $C_0 = 1.15$ and $\alpha_c = 0.68$ (obtained from flow visualization in the current work), x_c was determined from Eq. (3) and the resulting transition boundary is shown by dotted lines in Fig. 4a. The line provides a good prediction of the observed transition from bubbly to slug flow for microgravity flow. Similar approach was followed for $+1g$ and $-1g$ flows but using relevant drift flux models (see; Fig. 4b-d and Ayegba et al. (2022). The main difference in the bubbly (Bb)-intermittent (Sl/Ch) transition between μg and $+1g$ flows is α_c which is higher in the former. In the case of $-1g$ flow, bubbly flow was only observed for $G/\rho_l \geq 0.15\ m/s (G \geq 200 kg/m^2 s)$ and the transition from bubbly to intermittent flow occurred at higher α_c relative to both μg and $+1g$ flows. Furthermore in $-1g$ flow, an oscillating slug flow regime was observed for $G = 100 kg/m^2 s$ at high subcooling and low wall heat flux (Fig. 3 and Fig. 4).

By equating the void fraction computed from the slug flow model and that computed from the annular flow model, Dukler et al. (1988) proposed a critical void fraction (α_c) at transition from slug to annular flow in microgravity of 0.8. For μg-flow, x_c was determined from Eq. (3), $C_0 =$

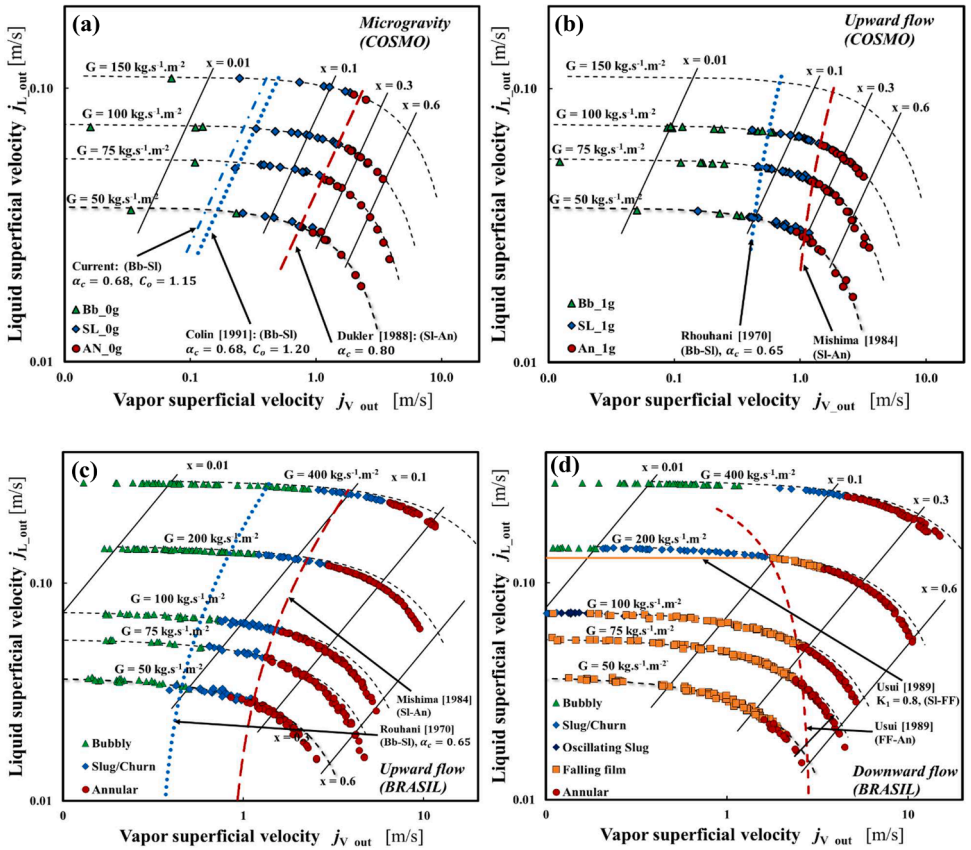

Fig. 4. Flow pattern map in a. μg flow, b & c. $+1g$ flow and d. -1g flow.

1.2 (Dukler et al., 1988) and the predicted transition boundary is shown by dotted curve in Fig. 4a. The curve provides a good prediction of the observed transition from intermittent to annular flow in microgravity. The effect of gravity on α_c at intermittent-annular flow transition was generally insignificant and the mean value of α_c was around 0.81 in all 3 gravity conditions. This value was used along with suitable intermittent-annular flow transition criteria such as those of Mishima and Ishii (1984) ($+1g$) and (Usui, 1989) ($-1g$) for the prediction of intermittent-annular flow transition in $+1g$ and $-1g$ flows (see Fig. 4b-d and Ayegba et al. (2022).

3.2. Heat transfer coefficient

3.2.1. Influence of mass flux and vapor quality on heat transfer coefficient

Fig. 5 shows measured heat transfer coefficient in microgravity flow along with those in upward and downward flows. In general, the measured heat transfer increased with mass flux in all 3 gravity conditions. At subcooled inlet conditions corresponding to nucleate boiling (NB) and bubbly flow, the heat transfer coefficient increased with vapor quality for all three gravity conditions and for the entire range of mass fluxes tested (Fig. 5). This vapor quality dependence sometimes stretched to the intermittent flow regime at low inlet vapor quality ($x_{in} < 0.1$). At saturated inlet conditions and for $G/\rho_l < 0.3\ m/s (G < 400 kg/m^2 s)$ bubble nucleation was observed in the annular film (NBA) (or falling film in downward flow NBFF) and the heat transfer coefficient was not particularly sensitive to changes in the vapor quality. It should be remarked that the falling film regime also occurred at subcooled inlet conditions with significant nucleation in the liquid film and little or no vapor quality dependence of the heat transfer coefficient. For $G/\rho_l \geq 0.3\ m/s, x \geq 0.35$ and $q''_w \leq 3\ W/cm^2$, no bubble nucleation was observed in the annular film and the measured heat transfer coefficient increased with vapor quality. This is due to decrease in film thickness with increase in vapor quality (Fig. 5b-c). It corresponds to the convective boiling regime (CB).

3.2.2. Influence of heat flux on heat transfer coefficient

Fig. 6 and Fig. 7 show the influence of heat flux on the measured heat transfer coefficient in microgravity flow along with those of upward and downward flows. In general, the measured heat transfer increased with heat flux in all 3 gravity conditions.

Microgravity heat transfer measurements were done using the COSMO experimental facility. For $50 \leq G \leq 150\ kg/m^2 s$, $0 \leq x \leq 0.6$ and $0.5 \leq q \leq 2.0\ W/cm^2$ nucleate boiling (NB) and nucleate boiling in the annular film (NBA) were the dominant mechanism of heat transfer and the measured heat transfer coefficient increased with heat flux (Fig. 6). Over the range of experimental conditions, the influence of heat flux decreased with mass flux and was quite independent of the vapor quality for saturated inlet conditions corresponding to annular flow. Selected results of measured heat transfer coefficient in $+1g$ obtained using both COSMO and BRASIL are also shown for reference (Fig. 7a) along with measured heat transfer in $-1g$ obtained using BRASIL (Fig. 7b). Similar heat flux dependence, as with μg, were recorded in $+1g$ and $-1g$. Heat transfer measurements in $+1g$ obtained using both experimental facilities were also in agreement which shows the reproducibility of the experiments (Fig. 7a). Additional heat transfer data in $+1g$ and $-1g$ was reported elsewhere (Ayegba et al., 2022).

4. Discussion and modelling

4.1. Influence of gravity on heat transfer coefficient

4.1.1. Microgravity (μg) and upward ($+1g$) flow boiling heat transfer coefficient

Fig. 8 provides a comparison between heat transfer coefficient in μg and $+1g$. In the range of mass and heat fluxes tested, there was very limited influence of gravity for $x \leq 0.05$. This agrees with the gravity-dependence map of Ohta et al. (2013) which was reproduced in dimensionless form to provide a scalable reference (Table 3). For $G = 50$ & $75\ kg/m^2 s$ gravity dependence was limited to $q < 1.5$ & $2 W/cm^2$ ($Bo < 0.002$) and $0.05 \leq x \leq 0.4$ (Fig. 8a-b). This again was in general agreement with Table 3, although Table 3 would suggest a limiting value of boiling number of $Bo < 0.0015$. For $G = 100\ kg/m^2 s$ gravity dependence was still observed for $q = 2 W/cm^2$ & $0.05 \leq x \leq 0.25$ (Fig. 8c). However, there was no gravity dependence for $q = 2 W/cm^2$ & $x > 0.25$. The microgravity data in the current work was limited to low mass fluxes ($G \leq 150\ kg/m^2 s$, $Re_{lo} = GD/\mu_l \approx 2000$), and the gravity dependence was mainly determined by the limiting value of boiling number of $Bo < 0.002$. The range of mass flux tested in the current work largely falls into the laminar flow regime ($Re_{lo} \leq 2000$). Under similar conditions of liquid Reynolds number, Lebon et al. (2019) also reported gravity dependence in terms of heat fluxes. The following inference were drawn from the current low mass flux ($Re_{lo} \leq 2000$) data.

1. For low Boiling number $Bo < 0.002$ (i.e., $G = 50\ kg/m^2 s$ & $q < 1.5 W/cm^2$, $G = 75\ kg/m^2 s$ & $q < 2.0 W/cm^2$, $G = 100\ kg/m^2 s$ & $q \leq 2.0 W/cm^2$) and $0.05 \leq x \leq 0.4$, there is low density of nucleated bubbles and limited interaction among nucleated bubbles. The frequency of bubble detachment from the heated wall was significantly influenced by gravity (buoyancy) and was higher in normal gravity relative to microgravity. Consequently, the measured heat transfer coefficient was higher in $+1g$ relative to μg.
2. For high Boiling number, $Bo > 0.002$ (i.e., $G = 50\ kg/m^2 s$ & $q \geq 1.5 W/cm^2$, $G = 75\ kg/m^2 s$ & $q \geq 2.0 W/cm^2$) and $0.05 \leq x \leq 0.4$, there is high density of nucleated bubbles and significant interaction among them. The frequency of bubble detachment from the heated wall was more influenced by bubble interaction and less influenced by gravity (buoyancy). Consequently, both the bubble detachment frequency and the measured heat transfer coefficients were similar in $+1g$ and μg.

High mass flux ($Re_{lo} > 2000$) microgravity data was reported in the Thesis of Narcy (2014). At high mass fluxes ($G \geq 200\ kg/m^2 s$, $Re_{lo} \geq 2700$) and high vapor qualities ($x \geq 0.3$), the ratio of inertia to buoyancy forces (Fr_m, Eq. (1) determines the gravity dependence of flow boiling heat transfer coefficient. According to Baba et al. (2012), flow boiling heat transfer coefficient becomes independent of gravity at mixture Froude number $Fr_m \geq 4$. It can be deduced from the Thesis of Narcy (2014) that in the convective dominant regime (corresponding to high Fr_m), the influence of the Boiling number Bo on gravity dependence diminishes. As seen in the current work and in the works of Lebon et al. (2019) and Ohta et al. (2013), the opposite is true for low mass fluxes (i.e., $Re_{lo} \leq 2000$) where the influence of the Boiling number Bo on gravity dependence is enhanced in Lebon et al. (2019) and Ohta et al. (2013).

Due to limitations of the existing gravity-dependence map, a gravity-dependence criterium was proposed in the current work. The proposed criterium combines the Bo threshold observed for $Re_{lo} \leq 2000$ with the Fr_m threshold of 4 proposed by Baba et al. (2012) which seems to be appropriate for $Re_{lo} \gg 2000$. In the proposed boundary (Eq. (4), the Bo threshold of 0.002 and the Fr_m threshold of 4 was combined in such a manner that the effect of the former is prominent at low mass fluxes (i.e., $Re_{lo} \leq 2000$) and low vapor qualities while the influence of the latter in prominent at high mass fluxes (i.e., $Re_{lo} \gg 2000$) and high vapor qualities.

$$Bo_{threshold} = 0.002 - \frac{0.002}{1 + e^{[-2(Fr_m - 2)]}} \tag{4}$$

The proposed criterium was applied to the current data, the data of Narcy (2014), Lebon et al. (2019) and Ohta et al. (2013). The proposed criterium accurately predicted the gravity-dependent regime of the

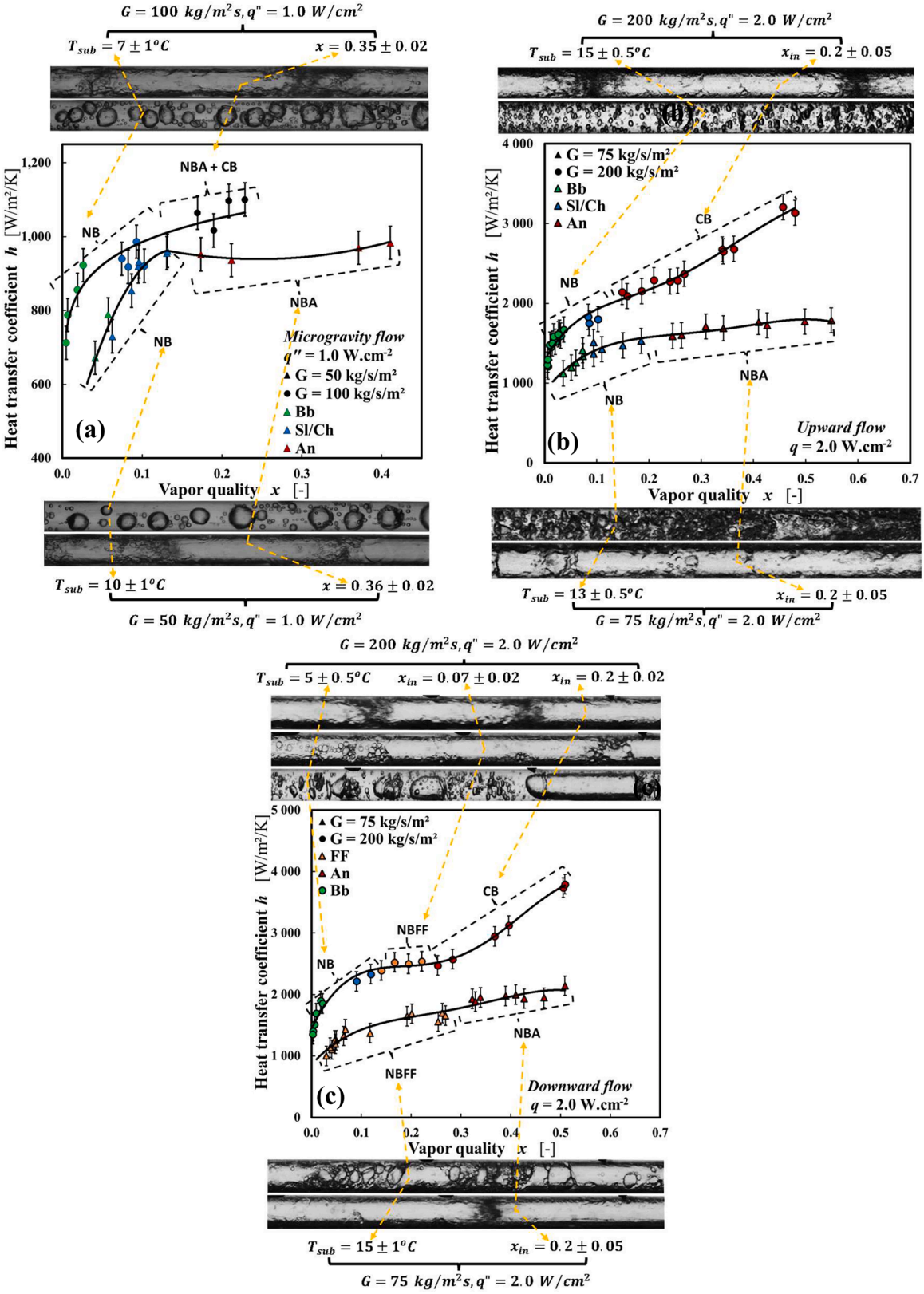

Fig. 5. Measured heat transfer coefficient versus vapor quality for selected mass fluxes, a. microgravity flow, b. upward flow, c. downward flow. NB; subcooled nucleate boiling. NBA; saturated nucleate boiling in the annular film. NBFF; subcooled or saturated nucleated boiling in the falling film. CB; saturated convective boiling. Solid lines are polynomial fits added to highlight trends.

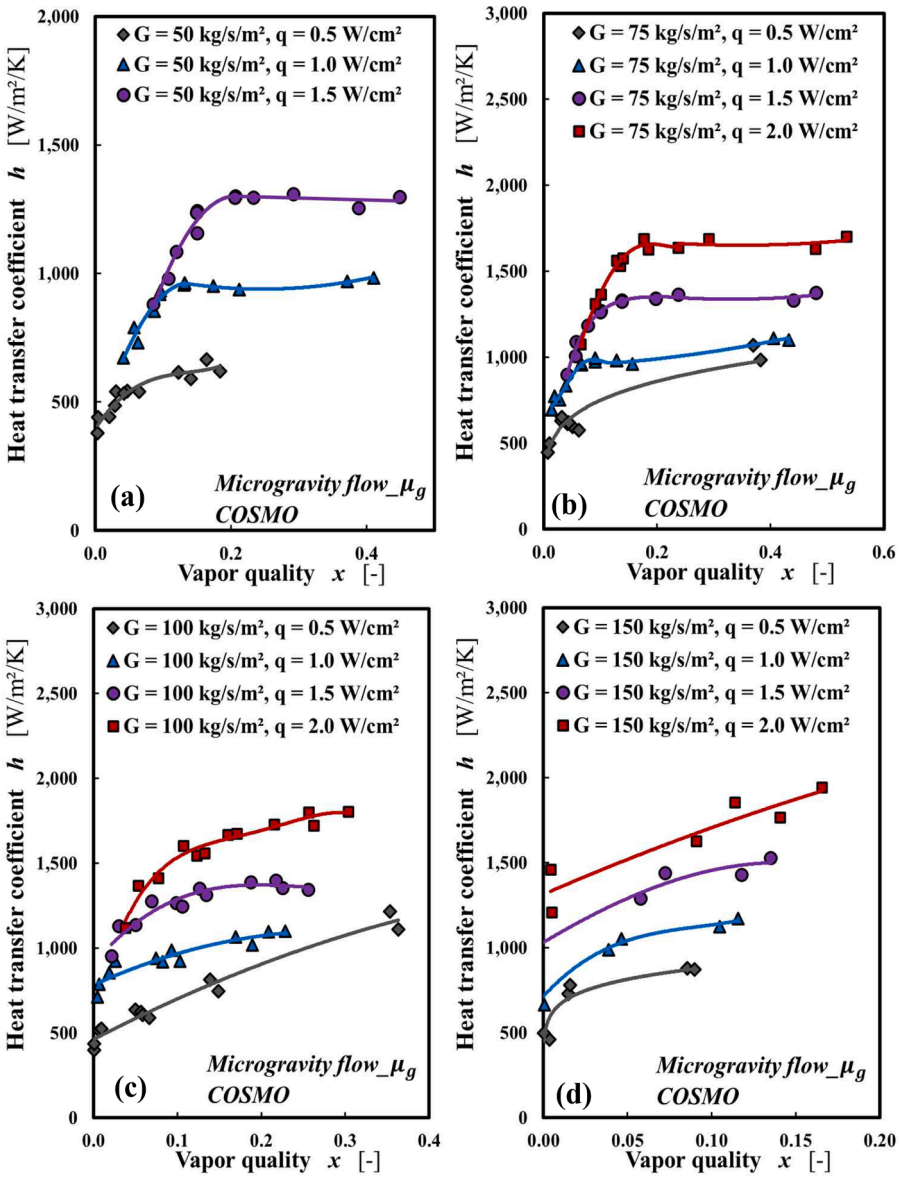

Fig. 6. Measured heat transfer coefficient versus vapor quality at selected heat fluxes in microgravity flow; a. $\boldsymbol{G = 50\ kg/m^2s}$, b. $\boldsymbol{G = 75\ kg/m^2s}$, c. $\boldsymbol{G = 100\ kg/m^2s}$, d. $\boldsymbol{G = 150\ kg/m^2s}$. The lines are trend lines of the experimental data and serve to provide clarity on the trends.

current work (Fig. 9a) and also correctly predicted the gravity-dependent regime for the data in the Thesis of Narcy (2014) in the range of $G > 75\ kg/m^2s$ (Fig. 9b). The proposed boundary failed to predict gravity-dependence for $G \leq 75\ kg/m^2s$ in the data of Narcy (2014). This could be associated to the high-thermal inertia of preheater used in the work of Narcy (2014). At low mass ($G > 75\ kg/m^2s$) the influence of the thermal inertia of the preheater becomes very important as the flow takes longer time to reach the desired test section inlet conditions. This could introduce some uncertainties in the vapor quality estimation at the inlet of the test section. In the current work, a very low thermal inertia preheater was used on the COSMO loop and heat loss estimation was also carried out. The proposed criterium also correctly predicted over 80 % and 92 % of the gravity-dependent/independent heat transfer data of Lebon et al. (2019) and Ohta et al. (2013) respectively (Fig. 9c). In the case of Ohta et al. (2013), the proposed criterium only failed to predict a few heat transfer data for $G = 150\ kg/m^2s$ (Fig. 9c). In the case of Lebon et al. (2019) the proposed criterium failed to predict a few heat transfer data for $G = 40,\ 80$ and $120\ kg/m^2s$ (Fig. 9c).

4.1.2. Microgravity (μg) and downward ($-1g$) flow boiling heat transfer coefficient

Fig. 10 provides a comparison between heat transfer coefficient in μg and $-1g$ for $50 \leq G \leq 100\ kg/m^2s$, $0 \leq x \leq 0.6$ and $0.5 \leq q \leq 2.0\ W/cm^2$. For low Boiling number ($Bo \leq 0.0024$: blue points in Fig. 10a, b & c and purple in Fig. 10b & c), the measured heat transfer coefficient was higher in $-1g$ relative to μg. For high Boiling number ($Bo > 0.0024$: purple in 8a), the measured heat transfer coefficients were similar in $-1g$ and μg or slightly higher in the latter. It should be remarked that for $G \leq 75\ kg/m^2s$ $\left(G/\rho_l \leq 0.056 ms^{-1}\right)$ in $-1g$ the flow pattern was mostly falling film regime and achieving flow stability was very difficult. Results of Fig. 10 also suggest that, the rate of increase in heat transfer coefficient with increase in the applied wall heat flux was slightly higher in μg relative to $-1g$ or of the same order of magnitude in both μg and $-1g$.

4.1.3. Upward ($+1g$) and downward ($-1g$) flow boiling heat transfer coefficient

Comparison of measured heat transfer in $+1g$ and $-1g$ for

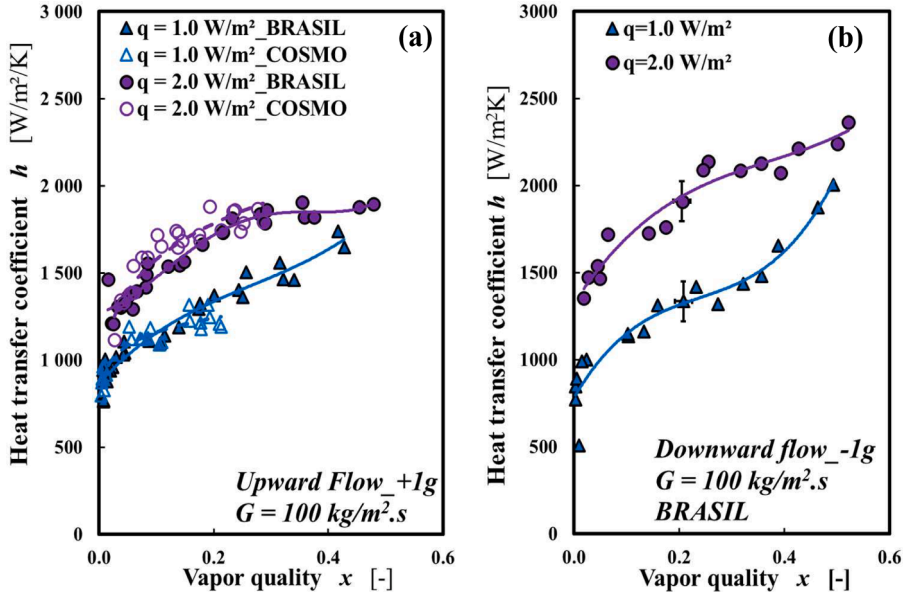

Fig. 7. Measured heat transfer coefficient versus vapor quality at $G = 100\ kg/m^2s$ and selected heat fluxes; a. upward flow ($+1g$) and b. downward flow ($-1g$). The lines are trend lines of the experimental data and serve to provide clarity on the trends.

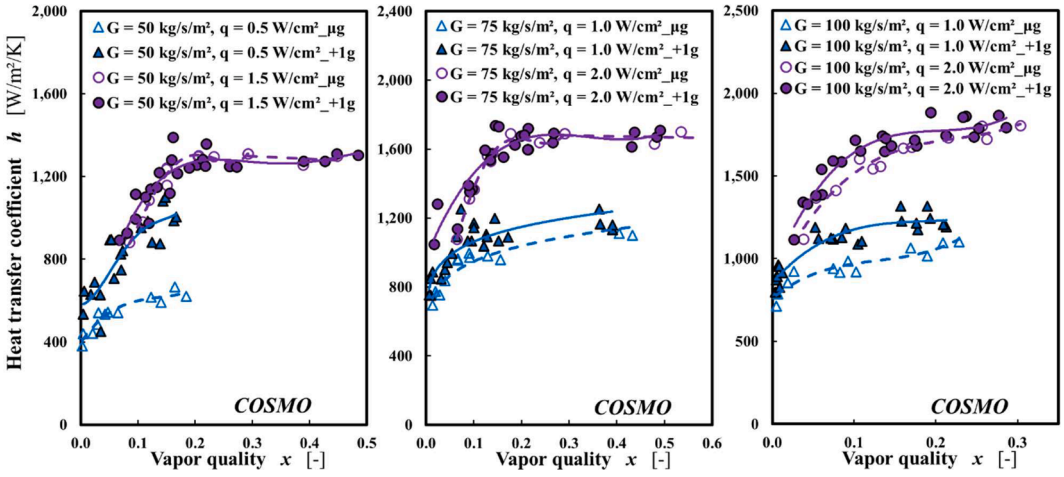

Fig. 8. Comparison between heat transfer coefficient in μg and $+1g$ flows. Solid lines are polynomial fits added to highlight trends.

Table 3
Gravity-dependence map for heat transfer coefficient of Ohta et al. (2013) reproduced in dimensional and dimensionless form.

		Low x	Moderate x	High x
$G \geq 300\ kg/m^2s$		No gravity effect	No gravity effect	No gravity effect
$50 \leq G \leq 200\ kg/m^2s$	$q" \geq 4\ W/cm^2$ $(Bo \geq 0.0015)$	Possible gravity effect	No gravity effect	No gravity effect
	$q" < 4\ W/cm^2$ $(Bo < 0.0015)$	Possible gravity effect	Gravity effect	No gravity effect
$G < 50\ kg/m^2s$		Possible gravity effect	No gravity effect	No gravity effect

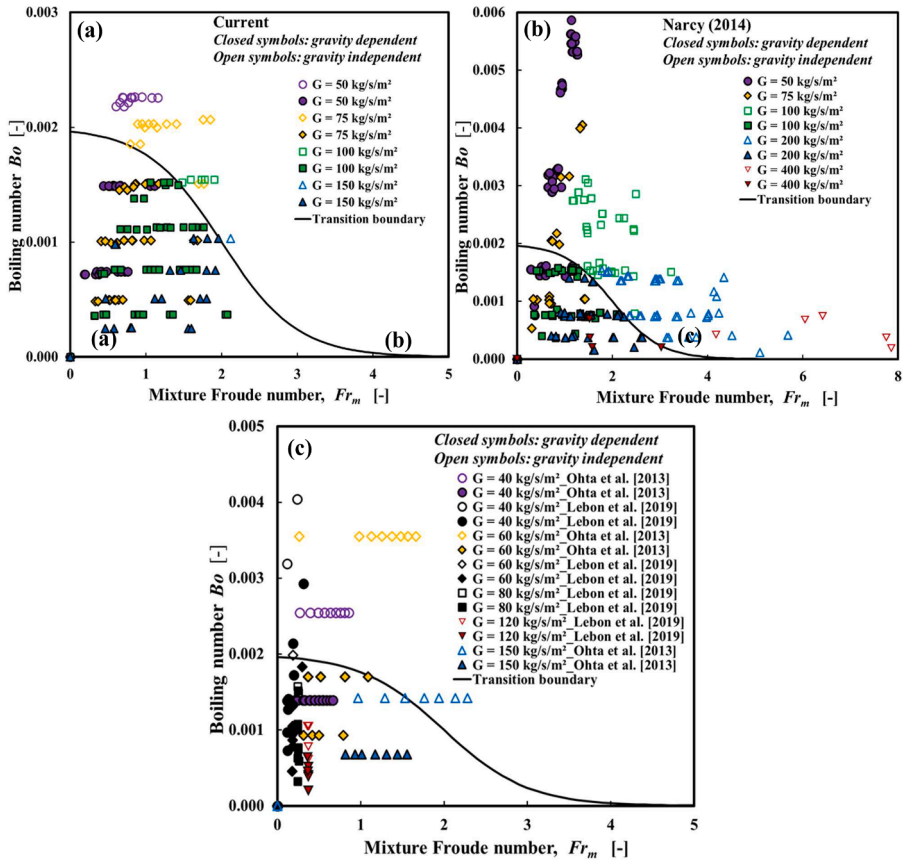

Fig. 9. Proposed gravity dependence map, a. current work, b. data of Narcy (2014), c. data of Lebon et al. (2019) and Ohta et al. (2013).

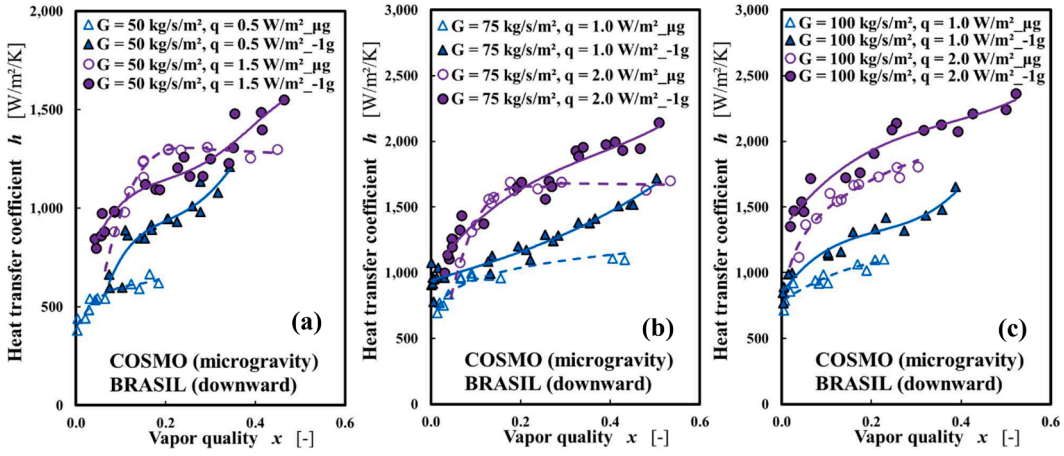

Fig. 10. Comparison between heat transfer coefficient in μg and $-1g$ flows. Solid lines are polynomial fits added to highlight trends.

$50 \leq G \leq 400\ kg/m^2s$, $0 \leq x \leq 0.7$ and $0.5 \leq q \geq 3.0\ W/cm^2$ was presented in Ayegba et al. (2022). For $G \geq 75\ kg/m^2s$ and $q \geq 0.5\ W/cm^2$, the measured heat transfer was higher in $-1g$ relative to $+1g$ and the difference ($h_{-1g} - h_{+1g}$) increased with heat flux. A similar trend was found when a comparison of τ_{w_-1g} and τ_{w_+1g} was done, although, the heat flux dependence of the wall shear stress was smaller relative to the heat flux dependence of the heat transfer coefficient. The coupling between the wall shear stress τ_w and the heat transfer coefficient h in both upward and downward flow was used as a bases for developing theoretical eddy viscosity models for the prediction of heat transfer coefficient in annular flow regime of upward and downward flows (Ayegba et al., 2023). Unfortunately, no wall shear stress measurements were performed in microgravity experiments. It was thus not conceivable to develop an eddy diffusivity model for the prediction of the heat transfer coefficient in microgravity.

4.2. Semi-empirical modelling of heat transfer coefficient in μg flow

In this section, a semi-empirical model for predicting the heat transfer coefficient in μg is proposed. Ayegba et al. (2022) proposed some modifications to the upward ($+1g$) flow boiling heat transfer model of (Kim and Mudawar (2013) to provide better representation of experimental trends in upward flow (Eq. (5). The model is valid for refrigerants flowing in smooth circular tubes in subcooled and saturated

conditions.

$$h_{2\varnothing} = \sqrt{\left(h_{nb}{}^2 + h_{cb}{}^2\right)} \tag{5}$$

$$h_{nb} = h_l\left[2345Bo^{0.76}\left(\frac{P}{P_{crit}}\right)^{0.38}(1-x)^{-0.7}\right] \tag{6}$$

$$h_{cb} = h_l\left[5.2Bo^{0.08}We_{lo}^{-0.54} + 5.1\left(\frac{1}{X_{tt}}\right)^{0.71}\left(\frac{\rho_v}{\rho_l}\right)^{0.13}\right] \tag{7}$$

$$Bo = \frac{q''}{Gh_{lv}}, X_{tt} = \left(\frac{1-x}{x}\right)^{0.9}\left(\frac{\rho_v}{\rho_l}\right)^{0.5}\left(\frac{\mu_l}{\mu_v}\right)^{0.1}, \; We_{lo} = G^2D\Big/(\sigma\rho_l),$$

$$h_l = 0.023Re_l^{0.8}Pr_l^{0.4}\frac{\lambda_l}{D}, \; Re_l = \frac{G(1-x)D}{\mu_l} \tag{8}$$

where Bo is the Boiling number, X_{tt} is the Lockhart–Martinelli parameter based on turbulent liquid-turbulent vapor flows, We_{lo} is the Weber number of the liquid, x is the vapor quality, P/P_{crit} is the reduced pressure, σ is the surface tension, Re_l is the liquid Reynolds number, h_l is determined from single-phase turbulent heat transfer correlation of Dittus and Boelter (1930).

Fig. 11 provides a comparison between measured and predicted (Eq. (5)), (Ayegba et al., 2022) heat transfer coefficient in $+1g$ flow. The proposed model predicted around 95 % of the measured data in $+1g$ within ±20% and reproduced the heat transfer evolution with mass flux, heat flux and vapor quality (Fig. 11f). Also, from the experimental data, it can be seen that, at low mass fluxes (for example, $G = 75\ kg/m^2s$, Fig. 11b) and $x \leq 0.6$, the heat transfer coefficient increases significantly with increase in wall heat flux. In these flow conditions, nucleate boiling (NB and NBA) is dominant over convective boiling heat transfer. At higher mass fluxes (for example, $G = 200\ kg/m^2s$, Fig. 11d) and $x \geq 0.35$, the measured heat transfer coefficient is quite independent of the wall heat flux and increases with vapor quality. In these flow conditions, convective boiling (CB) is dominant over nucleate boiling heat transfer. Interestingly, the model reproduced the parameter dependence of the measured heat transfer coefficient.

The focus of the current work is microgravity (μg) flow and there are no models for predicting $h_{2\varnothing\_\mu g}$. Owing to their better performance compared to other models in predicting $h_{2\varnothing\_+1g}$, the $h_{2\varnothing\_+1g}$ correlations of Kim and Mudawar (2013) and Ayegba et al. (2022) were tested for predicting the measured $h_{2\varnothing\_\mu g}$ in the current work as well as the measured $h_{2\varnothing\_\mu g}$ data in the work of Ohta et al. (2013) and the Thesis of Narcy (2014). As expected, both $h_{2\varnothing\_+1g}$ correlations overpredicted the $h_{2\varnothing\_\mu g}$ data in the current work and $h_{2\varnothing\_\mu g}$ data in the works of Ohta et al. (2013) and Narcy (2014) (Fig. 12). The modified $h_{2\varnothing\_+1g}$ correlation of Kim and Mudawar (2013) as given by Ayegba et al. (2022) (Fig. 12 bottom) provided a better prediction of the $h_{2\varnothing\_\mu g}$ database when compared to the original $h_{2\varnothing\_+1g}$ correlation of Kim and Mudawar (2013) (Fig. 12 top). Due to limitations of the $h_{2\varnothing\_+1g}$ correlations in predicting the measured $h_{2\varnothing\_\mu g}$, steps are taken in the current work to provide suitable correlation for predicting $h_{2\varnothing\_\mu g}$.

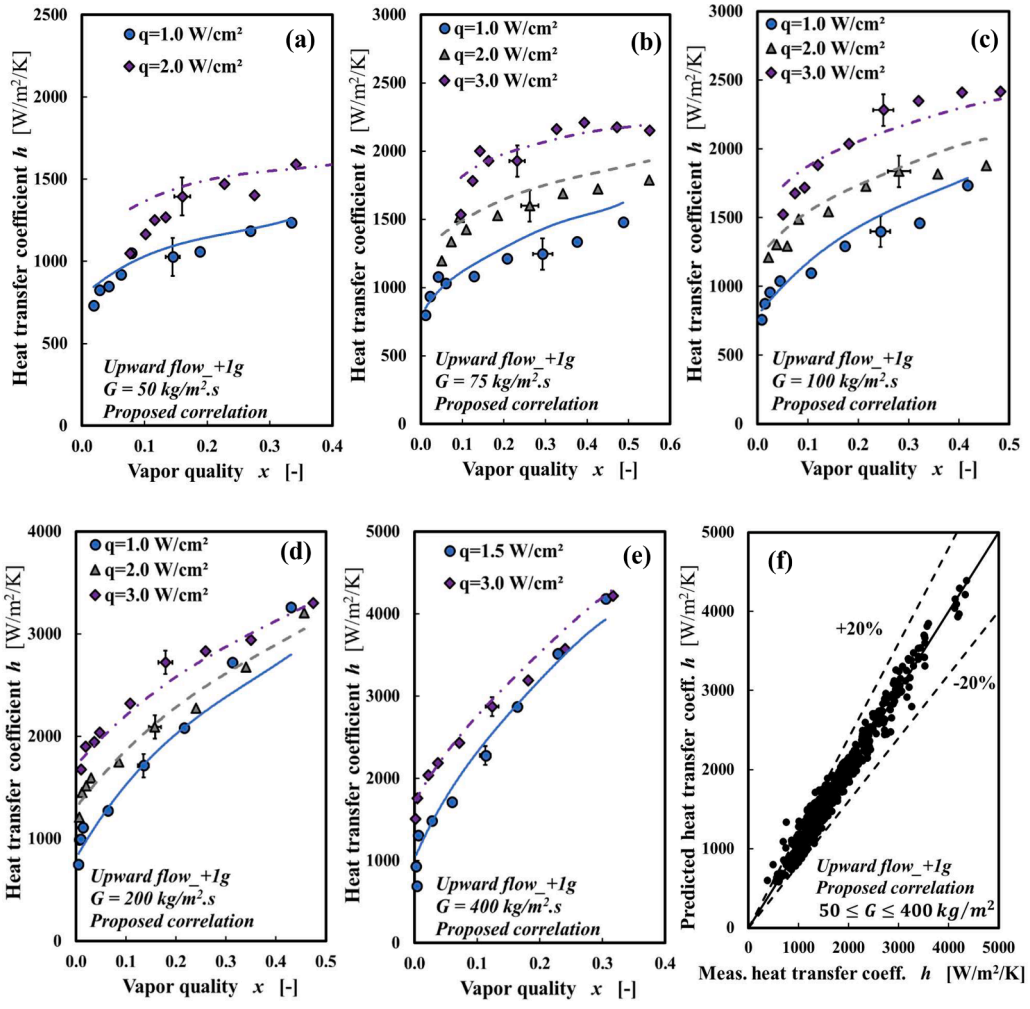

Fig. 11. Comparison of measured and predicted heat transfer coefficient in $+1g$ flow. Markers: experimental data. Lines: correlation.

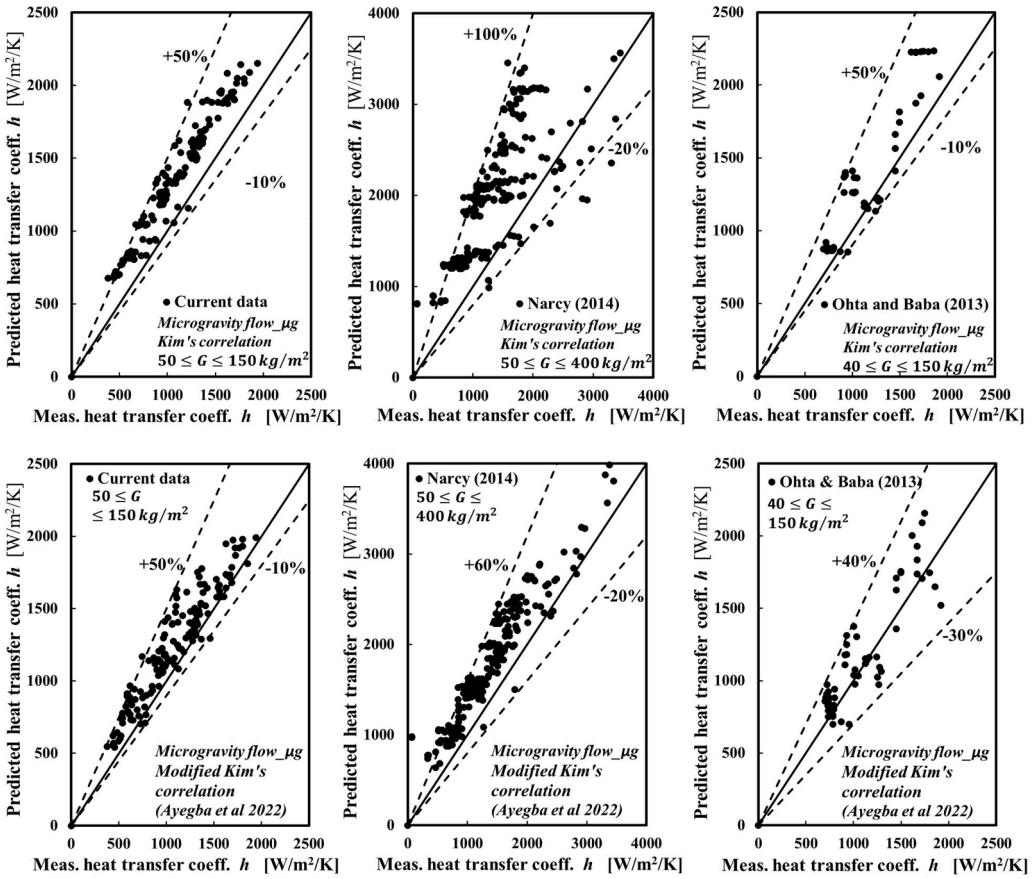

Fig. 12. Comparison of measured and predicted heat transfer coefficient in μg flow.

Some of the distinguishing features between $+1g$ and μg flows include:

1. Predominance of elongated bubbles (larger bubble sizes and higher void fraction) in μg relative to $+1g$ flows. This bubble characteristics is similar to the confined bubble growth observed in microchannels and results in the suppression of wall nucleation. The flow visualizations shown in Fig. 3 highlight this effect.
2. Thinner annular film (higher void fraction) in μg relative to $+1g$ flows. This enhances the drag effect of the vapor close to the wall. The thinner liquid film thickness reduces the thermal resistance of the liquid film.
3. Reduced wall and interfacial shear stress in μg relative to $+1g$ flows. In the PhD Thesis of Narcy (2014), the adiabatic wall shear stress of μg flow relative to $+1g$ flow $\tau_{w_{\mu g}}/\tau_{w_{+1g}}$ increased with mass flux and vapor quality from 30% to 100% . Ayegba et al. (2022) also showed that the influence on gravity decreased with mass flux and vapor quality. Furthermore, it was shown that in the fully convective regime at high mass flux, there was limited influence of gravity on the measured heat transfer, as it is the case for the wall shear stress. The dependence of $h_{2\varnothing}$ on $\tau_{w\_2\varnothing}$ would also suggest a similar trend for the convective part of the heat transfer coefficient (i.e., $h_{cb\_\mu g} = 30$ *to* 100% *of* h_{cb_+1g}).

It should be remarked that the effects of distinguishing features 1 and 2 (bubble size and liquid film thickness) are accounted for in distinguishing feature 3 (shear stress) through the two-phase momentum balance equation. Therefore, as a first step, a simple modification to the $h_{2\varnothing\_+1g}$ correlation of Ayegba et al. (2022) is done here in line with distinguishing feature 3. To account for this gravity dependence, a multiplier (F) was introduced to the convective part (h_{cb_+1g}) of the heat transfer correlation of Ayegba et al. (2022) (Eq. (7)) such that $h_{cb\_\mu g} = F.h_{cb\_+1g}$. F was determined as a simple power law function of the single-phase Reynolds number of the liquid (Re_{lo}) (Eq. (9), Fig. 13a).

$$F = 0.06Re_{lo}^{0.3} \quad (Re_{lo} = G.D/\mu_l) \tag{9}$$

Furthermore, it was remarked in the previous section, that the heat flux dependence in μg was higher than that in $+1g$ but of equivalent magnitude as that in $-1g$. In the current work, it was found that a 15 % increase in the nucleate boiling contribution to the total heat transfer coefficient was adequate to account for the higher heat flux dependence in μg relative to $+1g$ (i.e., $h_{nb\_\mu g} = 1.15 \times h_{nb\_+1g}$). This higher heat flux dependence is thought to be associated with the longer residence time and larger detachment diameter of nucleated bubbles on the wall in μg relative to $+1g$. The proposed model for predicting heat transfer coefficient in μg is therefore given by Eq. (10).

$$h_{2\varnothing\_\mu g} = \sqrt{\left[\left(1.15h_{nb\_+1g}\right)^2 + \left(F.h_{cb\_+1g}\right)^2\right]} \quad (microgravity\ flow) \tag{10}$$

Fig. 13 provides a comparison between measured (current work) and predicted (Eq. (10) heat transfer coefficient in μg flow. The proposed model predicted 100 % of the measured data in μg within ±20% and also reproduced the heat transfer evolution with mass flux, heat flux and vapor quality. The proposed model was also used to predict the measured μg heat transfer coefficient in the article of Ohta et al. (2013) and the measured μg heat transfer coefficient in the Thesis of Narcy (2014) (Fig. 14). The proposed model predicted nearly 100 % of the data of Ohta et al. (2013) within ±30% (Fig. 14a) and around 85 % of the data of Narcy (2014) within -20 % to +50 % (Fig. 14b).

Considering the similarities (elongated bubbles and thin annular liquid film) between microgravity flows and microchannel flows, a few correlations for heat transfer coefficient in cylindrical microchannel

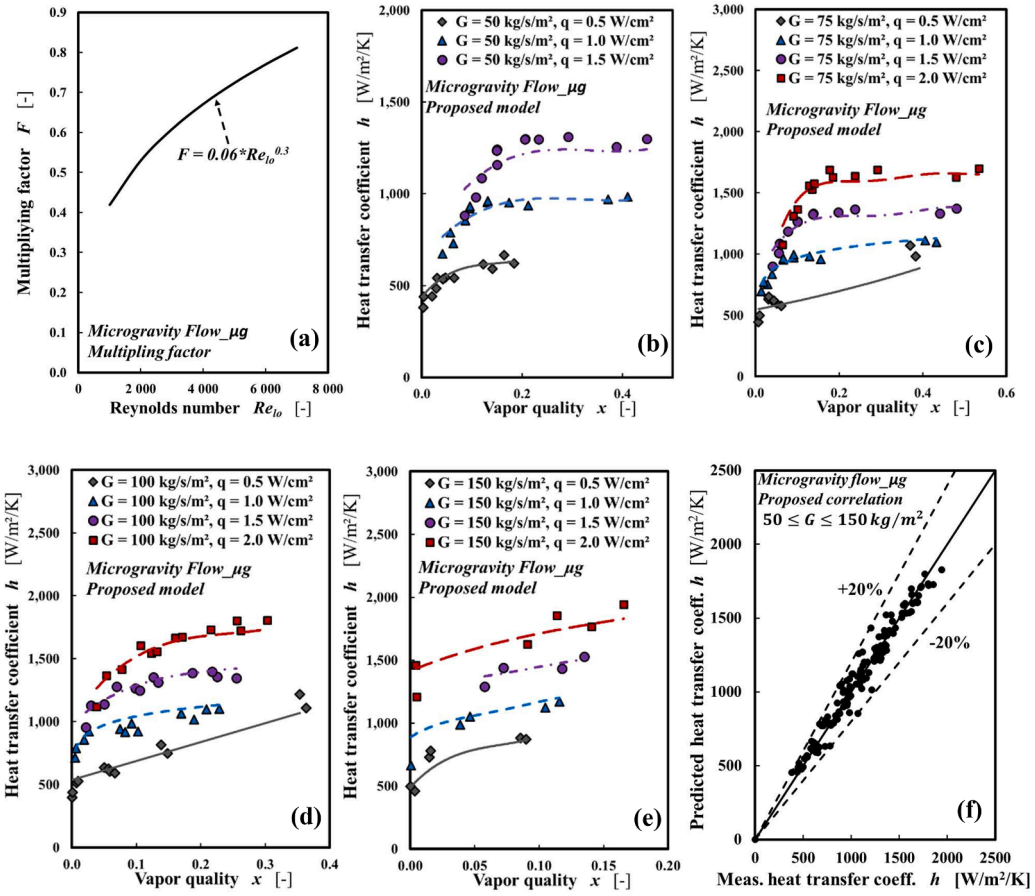

Fig. 13. Comparison between measured and predicted heat transfer coefficient in ***μg*** flow. Markers: current experimental data. Lines: correlation.

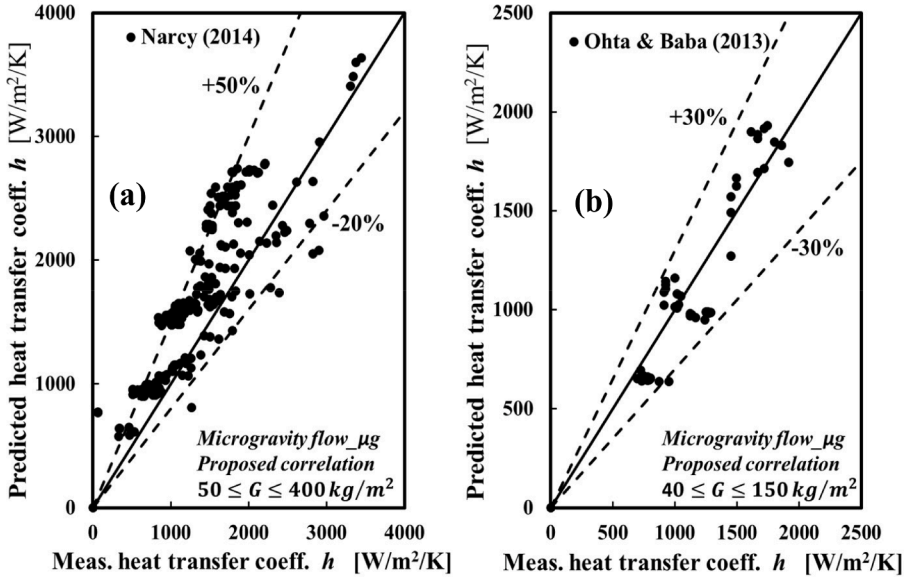

Fig. 14. Comparison between measured and predicted heat transfer coefficient in ***μg*** flow: a. data of Ohta et al. (2013), b. data in the PhD thesis of Narcy (2014).

flows were tested against the measured microgravity heat transfer coefficient (Basu et al., 2011; Costa-Patry et al., 2012; Kanizawa et al., 2016; Saitoh et al., 2007; Sun and Mishima, 2009; Zhang et al., 2004). In general, all the tested correlations failed to predict the measured $h_{2\varnothing-\mu g}$ for all three data sets. Among, the tested cylindrical microchannel correlations, the correlation of Kanizawa et al. (2016) provided the best reproduction of the parametric dependence (x, q'', G) of the measured $h_{2\varnothing-\mu g}$. The model however over-predicted the measure $h_{2\varnothing-\mu g}$ for all three data sets (See Fig. 15a for the current data set). Interestingly, for all three data sets and over the entire test conditions the over-prediction was by a factor of ≈ 1.72. Therefore, a simple multiplication of the microchannel heat transfer coefficient correlation of Kanizawa et al.

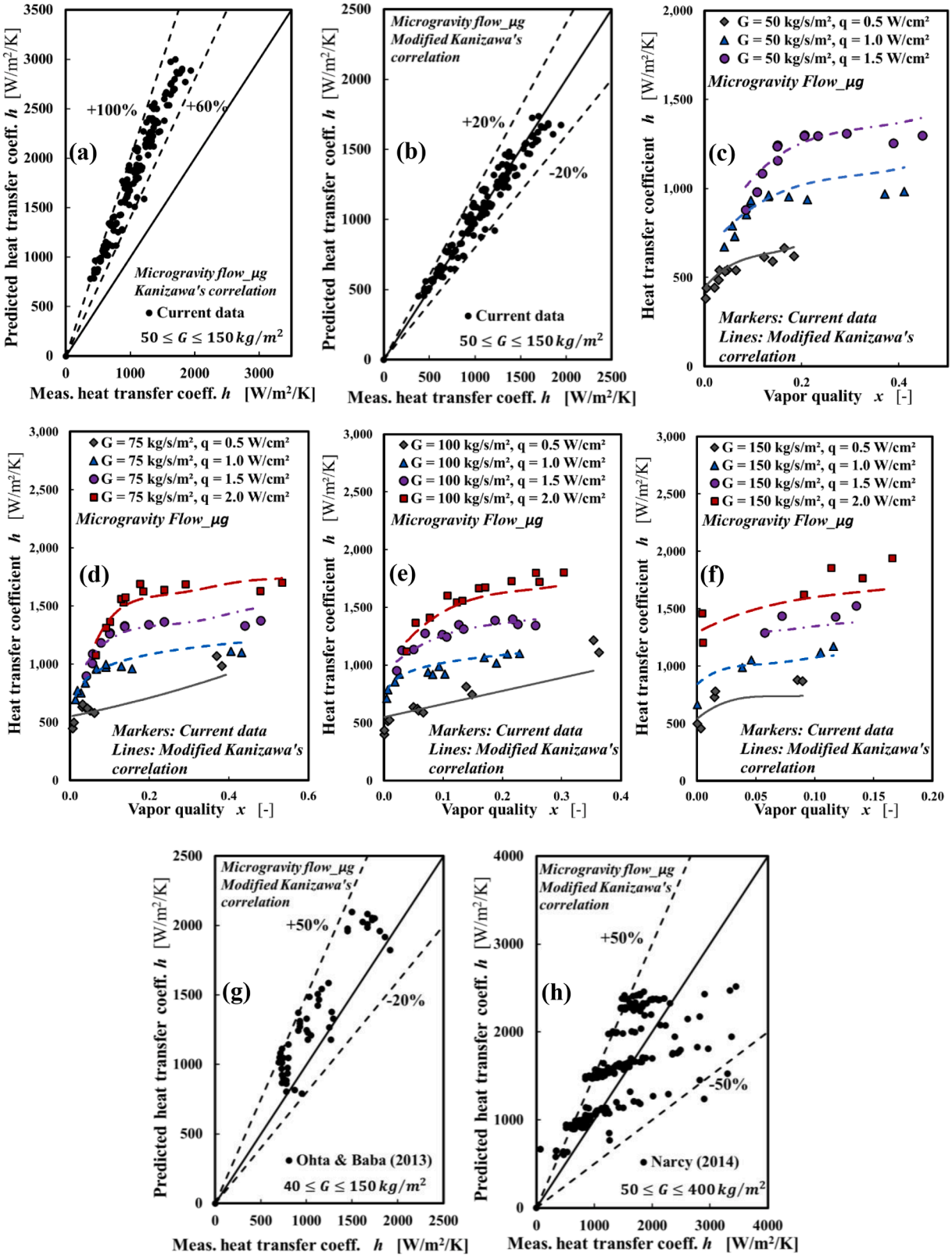

Fig. 15. a. Microchannel correlation of Kanizawa et al. (2016) vs current data, b. modified correlation of Kanizawa et al. (2016) vs current data, c-f. measured $h_{2\emptyset\_\mu g}$ and $h_{2\emptyset\_\mu g}$ predicted by the modified correlation of Kanizawa et al. (2016) vs vapor quality, g. modified correlation of Kanizawa et al. (2016) vs data of Ohta et al. (2013), h. modified correlation of Kanizawa et al. (2016) vs data in the PhD thesis of Narcy (2014).

(2016) by 0.58 (i.e., $h_{2\varnothing\_\mu g} = 0.58 h_{2\varnothing\_Kanizawa}$) provided very good predictions of the measured data for all three data sets (Fig. 15b-h). The modified correlation of Kanizawa et al. (2016) predicted 100 % of the current data within ±20% (Fig. 15b) and also reproduced the parametric trends (Fig. 15c-f). It also predicted about 100 % of the data of Ohta et al. (2013) within −20 & + 50% and the data of Narcy (2014) within ±50%.

$$h_{2\varnothing} = Sh_{nb} + Fh_{cb} \tag{11}$$

$$h_{nb} = 207\frac{\lambda_l}{d_b}\left(\frac{q'' d_b}{\lambda_l T_{sat}}\right)^{0.745}\left(\frac{\rho_v}{\rho_l}\right)^{0.581}(Pr_l)^{0.533} \tag{12}$$

$$h_{cb} = 0.023 Re_l^{0.8} Pr_l^{1/3}\frac{\lambda_l}{D} \tag{13}$$

$$F = 1 + \frac{2.5X^{-1.32}}{1 + We_{u_v}^{0.24}} \tag{14}$$

$$S = \frac{1.06Bd^{-8}\ \times 10^{-3}}{1 + 0.12\left(\frac{Re_{lo}F^{1.25}}{10000}\right)^{0.86}} \tag{15}$$

$$Bd = \frac{(\rho_l - \rho_v)D^2 g}{\sigma},\ We_{u_v} = \frac{\rho_v u_v^2 D}{\sigma},\ Re_v = \frac{GxD}{\mu_v},\ d_b = 0.51\sqrt{\frac{2\sigma}{g(\rho_l - \rho_v)}} \tag{16}$$

$$X_{tt} = \left(\frac{1-x}{x}\right)^{0.9}\left(\frac{\rho_v}{\rho_l}\right)^{0.5}\left(\frac{\mu_l}{\mu_v}\right)^{0.1} \quad for\ Re_v > 1000 \tag{17}$$

$$X_{tt} = \frac{1}{18.7}Re_v^{0.4}\left(\frac{1-x}{x}\right)^{0.9}\left(\frac{\rho_v}{\rho_l}\right)^{0.5}\left(\frac{\mu_l}{\mu_v}\right)^{0.1} \quad for\ Re_v > 1000 \tag{18}$$

$$\alpha = \left[1 + 1.025 Fr_m^{-0.092}\left(\frac{\rho_v}{\rho_l}\right)^{1/3}\left(\frac{\mu_l}{\mu_v}\right)^{-0.368}\left(\frac{1-x}{x}\right)^{2/3}\right]^{-1} \tag{19}$$

$$Fr_m = \frac{G^2}{(\rho_l - \rho_v)^2 gD},\ u_v = \frac{GD}{\rho_v \alpha} \tag{20}$$

$$h_{2\varnothing\_\mu g} = 0.58 h_{Kanizawa} \tag{21}$$

where F, S, d_b and T_{sat} are the convective boiling enhancement factor, nucleate boiling suppression factor, estimated bubble departure diameter, and the saturation temperature of the test fluid in Kelvin. Bd is the Bond number which was introduced to capture the influence of confined bubble growth on the suppression of nucleate boiling. We_{u_v} is the vapor Weber number based on the in-situ vapor velocity and account for the two-phase distribution along the cross-section.

5. Conclusions

This work explored the influence of gravity level as well as orientation relative to gravity on the flow pattern, void fraction, liquid film thickness, vapor velocity and heat transfer coefficient using experimental approach.

1. For $G/\rho_l \geq 0.15\ m/s$, bubbly, intermittent (slug/churn) and annular flow regimes were observed in $-1g$, μg and $+1g$ flows. For $G/\rho_l < 0.15\ m/s$ in $-1g$ flow, the bubbly flow regime was replaced by the falling film flow regime.
2. In general, the mean bubble and/or slug size decreased from $-1g$ flow through μg to $+1g$ in line with the bubble drift velocities associated with these gravity conditions. The opposite trend was observed with the liquid film thickness in the annular flow regime. Bubbles and/or slugs were more distorted in μg flow relative to both $+1g$ and $-1g$ flows due to the absence of buoyancy forces. The results of the current study along with those of Ayegba et al. (2022) and Narcy et al. (2014) leads to the conclusion that, the influence of gravity on bubble and/or slug geometry is limited to $G \leq 540\ kg/m^2s$ and/or $x \leq 0.35$.
3. Overall, the measured heat transfer coefficient in all three gravity conditions showed a dependence on heat flux, mass flux and/or vapor quality. The heat flux dependence was lower in $+1g$ flow relative to both μg and $-1g$ flows. For $Re_{lo} \leq 2000$ $(G \leq 150\ kg/m^2s)$ and $Bo < 0.002$ the measured heat transfer coefficient was highest in $-1g$ flow and lowest in μg flow but becomes comparable at $Bo \geq 0.002$. For $Re_{lo} \gg 2000$ $(G \gg 150\ kg/m^2s)$, gravity dependence was a function of both mass flux and vapor quality and becomes negligible at $G \geq 400\ kg/m^2s$ and/or $x \geq 0.35$.
4. Correlations for predicting heat transfer coefficient in microgravity were proposed in the current work. Suitable modification of the $h_{2\varnothing\_+1g}$ correlation of Ayegba et al. (2022) provided a correlation that predicted 100 % of the current μg data within ±20%. The correlation also predicted nearly 100 % of the μg data of Ohta et al. (2013) within ±30% and around 85 % of the μg data of Narcy (2014) within -20 % to +50 %. The correlation of Kanizawa et al. 2016 developed for circular micro-channel flows, multiplied by a factor 0.58 also provides good prediction of the heat transfer coefficient.
5. A simple correlation for predicting the gravity dependent regime as it relates to heat transfer coefficient in $+1g$ and μg flows was also proposed in this work. The proposed criterium correctly predicted over 85 % of the gravity-dependent heat transfer coefficient in the current work and the works of Lebon et al. (2019), Narcy (2014) and Ohta et al. (2013).

Authors statement

For Open Access, a CC-BY public copyright license has been applied by the authors to the present document and will be applied to all subsequent versions up to the Author Accepted Manuscript arising from this submission.

CRediT authorship contribution statement

Paul Onubi Ayegba: Writing – original draft, Visualization, Validation, Software, Methodology, Formal analysis, Data curation, Conceptualization. **Julien Sebilleau:** Writing – review & editing, Supervision, Software, Methodology, Investigation, Formal analysis, Data curation, Conceptualization. **Catherine Colin:** Writing – review & editing, Supervision, Resources, Project administration, Methodology, Investigation, Funding acquisition, Conceptualization.

Declaration of competing interest

The authors declare that they have no known competing financial interests or personal relationships that could have appeared to influence the work reported in this paper.

Data availability

Data will be made available on request.

Acknowledgement

Petroleum Technology Development Fund (PTDF) is acknowledged for the PhD grant funding of P. Ayegba. The European Space Agency (ESA) and the French Space Agency (CNES) through the GDR MFA are acknowledged for the financial support in the building of the experimental set-up and in the parabolic flight campaigns.

References

Ayegba, PO, Sebilleau, J, Colin, C., 2023. Theoretical modelling of heat transfer in vertical upward and downward annular flow boiling. Heat Transfer Eng. 1–22. https://doi.org/10.1080/01457632.2023.2191439.

Ayegba, PO, Sebilleau, J, Colin, C., 2022. Hydrodynamics of vertical upward and downward flow boiling in a millimetric tube. Internat. J. Multiphase Flow, 104120. https://doi.org/10.1016/j.ijmultiphaseflow.2022.104120.

Baba, S, Ohtani, N, Kawanami, O, Inoue, K, Ohta, H., 2012. Experiments on dominant force regimes in flow boiling using mini-tubes. Front. Heat Mass Transfer 3, 1–8. https://doi.org/10.5098/hmt.v3.4.3002.

Baltis, C, Celata, GP, Cumo, M, Saraceno, L, Zummo, G., 2012. Gravity influence on heat transfer rate in flow boiling. Microgravity. Sci. Technol. 24, 203–213. https://doi.org/10.1007/s12217-012-9298-5.

Basu, S, Ndao, S, Michna, GJ, Peles, Y, Jensen, MK., 2011. Flow boiling of R134a in circular microtubes—part i: study of heat transfer characteristics. J. Heat. Transfer. 133 https://doi.org/10.1115/1.4003159.

Bhagwat, SM, Ghajar, AJ., 2012. Similarities and differences in the flow patterns and void fraction in vertical upward and downward two phase flow. Exp. Therm. Fluid. Sci. 39, 213–227.

Celata, GP., 2007. Flow boiling heat transfer in microgravity: Recent results. Microgravity. Sci. Technol. 19, 13–17. https://doi.org/10.1007/BF02915738.

Celata, GP, Zummo, G., 2009. Flow boiling heat transfer in microgravity: recent progress. Multiphase Sci. Techn. 21, 187–212. https://doi.org/10.1615/multscientechn.v21.i3.20.

Chorin, P, Boned, A, Sebilleau, J, Colin, C, Schoele-Schulz, O, Picchi, N, et al., 2023. Conception of a compact flow boiling loop for the International Space Station- First results in parabolic flights. Comptes Rendus Mécanique 1–20.

Cioncolini, A, Thome, JR., 2011. Algebraic turbulence modeling in adiabatic and evaporating annular two-phase flow. Int. J. Heat. Fluid. Flow. 32, 805–817. https://doi.org/10.1016/j.ijheatfluidflow.2011.05.006.

Colin, C, Fabre, J, Dukler, AE., 1991. Gas-liquid flow at microgravity conditions-I. Dispersed bubble and slug flow. Internat. J. Multiphase Flow 17, 533–544. https://doi.org/10.1016/0301-9322(91)90048-8.

Costa-Patry, E, Olivier, J, jr, Thome, 2012. Heat transfer characteristics in a copper micro-evaporator and flow pattern-based prediction method for flow boiling in microchannels. Front. Heat Mass Transfer 3. https://doi.org/10.5098/hmt.v3.1.3002.

Dittus, E, Boelter, L., 1930. Experiments with fluid friction roughened pipes. Public. Eng. 2, 443.

Dukler, AE, Fabre, JA, McQuillen, JB, Vernon, R., 1988. Gas-liquid flow at microgravity conditions: Flow patterns and their transitions. Internat. J. Multiphase Flow 14, 389–400. https://doi.org/10.1016/0301-9322(88)90017-1.

Godbole, P V, Tang, CC, Ghajar, AJ., 2011. Comparison of void fraction correlations for different flow patterns in upward vertical two-phase flow. Heat Transfer Eng. 32, 843–860. https://doi.org/10.1080/01457632.2011.548285.

Hong, S, Wang, JX, Gao, Z, Dang, C., 2023. Review on state-of-the-art research in pool and flow boiling under microgravity. Exp. Therm. Fluid. Sci. 144 https://doi.org/10.1016/j.expthermflusci.2023.110848.

Iceri, DM, Zummo, G, Saraceno, L, Ribatski, G., 2020. Convective boiling heat transfer under microgravity and hypergravity conditions. Int. J. Heat. Mass Transf. 153 https://doi.org/10.1016/j.ijheatmasstransfer.2020.119614.

Kandlikar, SG., 1990. A general correlation for saturated two-phase flow boiling heat transfer inside horizontal and vertical tubes. J. Heat. Transfer. 112, 219–228. https://doi.org/10.1115/1.2910348.

Kanizawa, FT, Tibiriçá, CB, Ribatski, G., 2016. Heat transfer during convective boiling inside microchannels. Int. J. Heat. Mass Transf. 93, 566–583. https://doi.org/10.1016/j.ijheatmasstransfer.2015.09.083.

Kharangate, CR, O'Neill, LE, Mudawar, I, 2016. Effects of two-phase inlet quality, mass velocity, flow orientation, and heating perimeter on flow boiling in a rectangular channel: Part 1 – Two-phase flow and heat transfer results. Int. J. Heat. Mass Transf. 103, 1261–1279. https://doi.org/10.1016/j.ijheatmasstransfer.2016.05.060.

Kim, SM, Mudawar, I., 2013. Universal approach to predicting saturated flow boiling heat transfer in mini/micro-channels – Part II. Two-phase heat transfer coefficient. Int. J. Heat. Mass Transf. 64, 1239–1256. https://doi.org/10.1016/j.ijheatmasstransfer.2013.04.014.

Konishi, C, Lee, H, Mudawar, I, Hasan, MM, Nahra, HK, Hall, NR, et al., 2015. Flow boiling in microgravity: Part 1 - Interfacial behavior and experimental heat transfer results. Int. J. Heat. Mass Transf. 81, 705–720. https://doi.org/10.1016/j.ijheatmasstransfer.2014.10.049.

Konishi, C, Mudawar, I., 2015. Review of flow boiling and critical heat flux in microgravity. Int. J. Heat. Mass Transf. 80, 469–493. https://doi.org/10.1016/j.ijheatmasstransfer.2014.09.017.

Lebon, MT, Hammer, CF, Kim, J., 2019. Gravity effects on subcooled flow boiling heat transfer. Int. J. Heat. Mass Transf. 128, 700–714. https://doi.org/10.1016/j.ijheatmasstransfer.2018.09.011.

Luciani, S, Brutin, D, le Niliot, C, Rahli, O, Tadrist, L., 2008. Flow boiling in minichannels under normal, hyper-, and microgravity: local heat transfer analysis using inverse methods. J. Heat. Transfer. 130, 101502 https://doi.org/10.1115/1.2953306.

Luciani, S, Brutin, D, Le, Niliot C, Tadrist, L, Rahli, O, 2009. Boiling heat transfer in a vertical microchannel: local estimation during flow boiling with a non intrusive method. Multiphase Sci. Techn. 21, 297–328. https://doi.org/10.1615/multscientechn.v21.i4.30.

Lui, R, Kawaji, M, Ogushi, T., 1994. An Experimental investigation of subcooled flow boiling heat transfer under microgravity conditions. In: Proc. 10th Int. Heat Transfer Conf. Brighton, UK, pp. 497–502.

Ma, Y, Chung, JN., 2001. A study of bubble dynamics in reduced gravity forced-convection boiling. Int. J. Heat. Mass Transf. 44, 399–415. https://doi.org/10.1016/s0017-9310(00)00106-x.

Mishima, K, Ishii, M., 1984. Flow regime transition criteria for upward two-phase flow in vertical tubes. Int. J. Heat. Mass Transf. 27, 723–737. https://doi.org/10.1016/0017-9310(84)90142-X.

Mudawar, I, Lee, J., 2023. Experimental and computational investigation into hydrodynamic and heat transfer characteristics of subcooled flow boiling on the international space station. Int. J. Heat. Mass Transf. 207, 124000 https://doi.org/10.1016/j.ijheatmasstransfer.2023.1240.

Narcy, M., 2014. PhD Thesis Institut National Polytechnique de Toulouse. https://doi.org/10.1017/CBO9781107415324.004.

Narcy, M, Colin, C., 2015. Two-phase pipe flow in microgravity with and without phase change: recent progress and future prospects. Interfacial. Phenom. Heat. Transf. 3, 1–17. https://doi.org/10.1615/interfacphenomheattransfer.2015012413.

Narcy, M, de Malmazet, E, Colin, C, 2014. Flow boiling in tube under normal gravity and microgravity conditions. Internat. J. Multiphase Flow 60, 50–63. https://doi.org/10.1016/j.ijmultiphaseflow.2013.11.011.

Ohta, H., 1997. Experiments on microgravity boiling heat transfer by using transparent heaters. Nuclear Eng. Design 175, 167–180. https://doi.org/10.1016/S0029-5493(97)00172-6.

Ohta, H, Baba, S, Asano, H, Kawanami, O, Suzuki, K, Fujii, K., 2013. Subjects to be clarified in flow boiling experiments on board international space station. In: 8th International conference on multiphase flow ICMF 2013. Jeju, Korea, pp. 1–13. https://doi.org/10.13140/2.1.1374.6565.

Saito, M, Yamaoka, N, Miyazaki, K, Kinoshita, M, Abe, Y., 1994. Boiling two-phase flow under microgravity. Nuclear Eng. Design 146, 451–461. https://doi.org/10.1016/0029-5493(94)90350-6.

Saitoh, S, Daiguji, H, Hihara, E., 2007. Correlation for boiling heat transfer of R-134a in horizontal tubes including effect of tube diameter. Int. J. Heat. Mass Transf. 50, 5215–5225. https://doi.org/10.1016/j.ijheatmasstransfer.2007.06.019.

Sun, L, Mishima, K., 2009. An evaluation of prediction methods for saturated flow boiling heat transfer in mini-channels. Int. J. Heat. Mass Transf. 52, 5323–5329. https://doi.org/10.1016/j.ijheatmasstransfer.2009.06.041.

Trejo-Peimbert, E., 2018. Dynamics and transfers in two phase flows with phase change in normal and microgravity conditions. Institut National Polytechnique de Toulouse. PhD Thesis.

Usui, K., 1989. Vertically downward two-phase flow, (II): Flow regime transition criteria. J. Nucl. Sci. Technol. 26, 1013–1022. https://doi.org/10.1080/18811248.1989.9734422.

Zhang, W, Hibiki, T, Mishima, K., 2004. Correlation for flow boiling heat transfer in mini-channels. Int. J. Heat. Mass Transf. 47, 5749–5763. https://doi.org/10.1016/j.ijheatmasstransfer.2004.07.034.